SCIENCE CHINA
Information Sciences

• RESEARCH PAPER •

October 2024, Vol. 67, Iss. 10, 202301:1–202301:16
https://doi.org/10.1007/s11432-024-4102-3

Weighted sum power maximization for STAR-RIS-aided SWIPT systems with nonlinear energy harvesting

Weiping SHI[1], Cunhua PAN[2], Feng SHU[3,4*], Yongpeng WU[5], Jiangzhou WANG[6], Yongqiang BAO[7] & Jin TIAN[8]

[1]*School of Network and Communication, Nanjing Vocational College of Information Technology, Nanjing* 210023*, China;*
[2]*National Mobile Communications Research Laboratory, Southeast University, Nanjing* 211189*, China;*
[3]*School of Information and Communication Engineering, Hainan University, Hainan* 570228*, China;*
[4]*School of Electronic and Optical Engineering, Nanjing University of Science and Technology, Nanjing* 210094*, China;*
[5]*Shanghai Key Laboratory of Navigation and Location Based Services, Shanghai Jiao Tong University, Shanghai* 200240*, China;*
[6]*School of Engineering, University of Kent, Canterbury* CT2 7NT*, UK;*
[7]*School of Information and Communication Engineering, Nanjing Institute of Technology, Nanjing* 211167*, China;*
[8]*Engineering School of Networks and Telecommunications, Jinling Institute of Technology, Nanjing* 211169*, China*

Received 24 January 2024/Revised 21 May 2024/Accepted 17 July 2024/Published online 13 September 2024

Abstract The conventional reconfigurable intelligent surface (RIS) is limited to reflecting incident signals, thereby imposing constraints on the placement of the transmitter and receiver, which hinders achieving comprehensive signal coverage across an entire area. This paper investigates a simultaneously transmitting and reflecting (STAR)-RIS-aided simultaneous wireless information and power transfer (SWIPT) system with a nonlinear energy harvesting model under three different RIS transmission protocols: energy splitting (ES), time switching (TS), and mode switching (MS). The objective of this paper is to maximize the weighted sum power (WSP) of all energy harvesting receivers (EHRs) while ensuring fairness in the collected power among them. This is achieved by jointly optimizing the transmit beamforming at the base station (BS) and the transmission and reflection coefficients at the STAR-RIS, subject to rate constraints for information decoding receivers (IDRs), transmit power constraint at the BS, and coefficient constraints of each element at the STAR-RIS corresponding to the three protocols. Solving this optimization problem poses challenges because of the complicated objective function and numerous coupled optimization variables of the ES STAR-RIS. To address this complexity, an efficient alternating optimization (AO) approach is proposed as an iterative solution method that achieves suboptimal results. The AO algorithm is then extended to MS STAR-RIS and TS STAR-RIS. Specifically, for MS STRA-RIS, binary constraints in the STAR-RIS coefficient optimization subproblem are handled using the first-order approximation technique along with the penalty function method. For TS STAR-RIS, apart from optimizing BS transmit beamforming and STAR-RIS coefficients subproblems, the transmission and reflection time allocation of STAR-RIS also needs optimization. Numerical findings demonstrate that compared to conventional RIS-aided systems, utilizing three different protocols in a STAR-RIS-aided system can enhance power collection at EHRs while expanding the receiver placement range. Furthermore, TS STAR-RIS performs best when the IDRs do not require high achieved rates. Otherwise, ES is the best choice.

Keywords STAR-RIS, beamforming, SWIPT, alternating optimization, nonlinear energy harvesting

1 Introduction

In recent years, with the tremendous growth of the Internet of Things, wireless communication technologies, and the large-scale popularization of smart devices in people's lives, the amount of user equipment and the flow of mobile data have grown exponentially [1–4]. The ever-increasing demand for data and the dramatic growth in the number of wirelessly linked devices exacerbate the problems of spectrum resource shortage and energy shortage [5]. Using radio frequency (RF) signals to implement the simultaneous

* Corresponding author (email: shufeng0101@163.com)

transfer of information and energy is an important means to solving the problem of energy limitation in wireless networks and achieving green communication [6–8]. However, in practice, energy harvesting receivers (EHRs) usually require higher reception power than information decoding receivers (IDRs) because of the difference between them in reception sensitivity and application requirements. Therefore, the inefficiency of the long-range wireless power transfer (WPT) of EHRs is regarded as a capability barrier for current simultaneous wireless information and power transfer (SWIPT) systems. Large-scale multiple-input multiple-output (MIMO) techniques could significantly boost WPT efficiency by arranging enormous arrays at the transmitters and receivers, but their practical implementation is still hindered by high hardware costs, complexity, and energy consumption [9–11].

Reconfigurable intelligent surfaces (RISs) offer a good approach to overcoming the aforementioned communication restrictions [12–14]. In particular, a RIS is made up of numerous inexpensive passive components that are controlled by intelligent controllers to adjust the phase shift of the incident signal, thereby boosting the receiver's signal intensity [15]. In contrast to conventional multiantenna technologies and relays, which employ pricey RF chains to actively create wireless signals, RISs simply passively reflect arriving signals back into the network, eliminating the need to configure RF chains and making the system more environmentally friendly and economical [16–18]. Given the various advantages of RIS, RIS-aided communication systems have gained widespread attention [12, 15, 16, 18–20].

However, most of the current research concerned with RISs addresses only reflected signal functions. In this case, the positions of the transmitters and receivers are limited in that they can only be located on the same side of the RIS. Otherwise, the receivers cannot receive the reflected signals. Such geographical restrictions may not always be satisfactory [21]. The RIS with entirely reflected signals significantly restricts the flexibility and efficiency of the system since the transmitters and receivers could be situated on either end of the RIS to address the issues mentioned above. Researchers came up with the notion of simultaneously transmitting and reflecting (STAR)-RISs [21]. Specifically, the radio signal transmitted to each STAR-RIS unit from one side is split into two distinct parts: the transmission part and the reflection part. The signal in the transmission part is transmitted to the space opposite the incident signal, while the signal in the reflection part is reflected to the same space as the incident signal. The transmission and reflection coefficients (TARCs) may be utilized to reconfigure the transmission and reflection signals, respectively, by varying the current and magnetic current of each STAR-RIS element. It should be emphasized here that the TARCs are two independent coefficients [22]. In addition, with STAR-RIS, signal coverage, signal freedom, and building compatibility can all be improved [23].

Many studies have been carried out on RIS-aided SWIPT systems to enhance their performance, which includes transmit power (TP) [24], received power of EHR, achieved rate of IDR [25, 26], and system security performance [27, 28]. Specifically, a multiple RIS-aided SWIPT system was researched in order to reduce the TP at the base station (BS) while meeting energy harvesting requirements at the EHRs and individual signal-to-interference-plus-noise ratio (SINR) requirements at each IDR [24]. An effective iterative technique based on the penalty method was proposed to solve the non-convex optimization problem for TP reduction. A RIS-aided SWIPT system was taken into consideration to boost the weighted sum power (WSP) that EHRs received [25]. The authors also showed that arbitrary user channels in the SWIPT system did not require particular energy signals. An RIS-aided MIMO-SWIPT system was developed to raise the weighted sum rate of IDRs [26]. In [27], one RIS was introduced into a secure SWIPT system to enhance its security. The semidefinite relaxation (SDR)-based alternating optimization (AO) technique and low complexity AO approach were employed to enhance active and passive beamforming. Furthermore, RIS was employed in secure MIMO-SWIPT systems to jointly optimize RIS phase shifts, artificial noise (AN) covariance, and precoding matrices with the goal of raising the secrecy rate of the system [28].

The RIS in the aforementioned RIS-aided systems solely serves the purpose of reflecting incident signals. Such RIS-aided systems fail to achieve complete coverage of reflected signals. A concept called STAR-RIS was made to greatly enhance the coverage capability of RIS and boost flexibility in transmitter and receiver placement. In particular, Ref. [22] presented the fundamental signal model for STAR-RIS and detailed energy splitting (ES), mode switching (MS), and time switching (TS) protocols employed by STAR-RIS. Furthermore, optimization techniques were applied to minimize power consumption in STAR-RIS-aided communication systems. Additionally, in STAR-RIS-aided systems, Ref. [29] offered channel models for both near-field and far-field scenarios. The authors also derived a closed-form expression for channel gain experienced by users who receive transmitted and reflected signals. Ref. [22] investigated a unicast/multicast communication system facilitated by STAR-RIS as a means of reducing the TP of the

BS. Additionally, an AO-based iterative technique was used to optimize the secrecy rate, which led to the creation of a secure non-orthogonal multiple access system backed by STAR-RIS [30]. These different publications show that STAR-RIS greatly improves overall performance when added to current systems. These various examples demonstrate that incorporating STAR-RIS into existing systems significantly enhances overall performance levels.

Most current papers have only studied conventional RIS-aided SWIPT systems. However, conventional RISs limit the freedom of location of EHRs. This paper exploits the potential of STAR-RIS in enhancing SWIPT systems where multiple EHRs and IDRs are situated on each side of the STAR-RIS in order to improve the receiving power and placement range of EHRs in SWIPT systems. In addition, it employs the nonlinear energy harvesting model to study the STAR-RIS-aided SWIPT system while accounting for the nonlinear features of end-to-end energy conversion in real energy harvesting circuits. To the best of our knowledge, similar work has not been extensively pursued. An overview of our primary contributions is provided below.

(1) The system under consideration is the SWIPT system assisted by STAR-RIS and modeled with nonlinear energy harvesting. We formulate the WSP maximization issue at the EHRs under three operating protocols (ES, MS, TS). The transmit beamforming at the BS and the transmission and reflection beamforming at the STAR-RIS are designed concurrently. Furthermore, it ensures the power constraint of the BS, the TARCs constraint of each element at the STAR-RIS, and the achieved rate requirements of the IDRs. However, because of the complexity introduced by the nonlinear energy harvesting model expression and coupling between multiple optimization variables, obtaining an optimal solution with a closed-form expression becomes a challenge.

(2) For the ES STAR-RIS case, we first convert the original optimization problem into an equivalent problem by introducing relaxation variables and adding corresponding constraints to represent objective function requirements. Since there is coupling among optimization variables and non-convexity in constraints, we decompose this problem into two subproblems: optimizing BS transmit beamforming and optimizing STAR-RIS transmission/reflection beamforming. We optimize these two subproblems using the AO algorithm. For each subproblem, the non-convex constraints are transformed into convex constraints by employing a first-order Taylor expansion approach. Next, the interior point technique is used to find the optimal solution to the subproblem.

(3) Additionally, our proposed iteration-based AO approach is expanded for the MS STAR-RIS case, which involves a mixed-integer non-convex optimization issue, and the TS STAR-RIS case, which involves a generic non-convex optimization problem. Specifically, for the MS STAR-RIS transmission/reflection coefficient optimization subproblem, the integer non-convex optimization problem is converted into a continuous convex optimization problem based on the penalty function method and the first-order approximation technique. Then, an iterative algorithm based on the successive convex approximation technique is proposed to find the proximate optimum solution. For TS STAR-RIS, similar to ES STAR-RIS, the suboptimal solution is obtained by alternately optimizing three subproblems in an iterative manner.

(4) Numerical findings show that the proposed STAR-RIS-aided SWIPT system can accomplish greater power harvesting at EHRs and broaden the location of EHRs in comparison to traditional RIS-aided systems. In addition, the TS protocol is superior for a lower achieved rate of IDRs. However, for a higher achieved rate of IDRs, the ES protocol performs best.

The remainder of this study is divided into the following sections. In Section 2, the system model and the formulation of the problem are presented; in Section 3, an effective approach for concurrently developing transmit beamforming and TARCs in ES STAR-RIS is proposed; Section 4 provides optimization designs for MS STAR-RIS and TS STAR-RIS; Section 5 analyzes the convergence of the three algorithms and calculates their computational complexities; Section 6 presents numerical results outcomes that illustrate the effectiveness of the three suggested STAR-RIS-aided SWIPT designs compared to the baseline plan; Section 7 concludes the article.

2 System model and problem formulation

2.1 System model

Figure 1 depicts a SWIPT system aided by a STAR-RIS, consisting of a BS with M antennas, K single-antenna IDRs, L single-antenna EHRs, and a STAR-RIS with N elements. The sets of IDRs, EHRs,

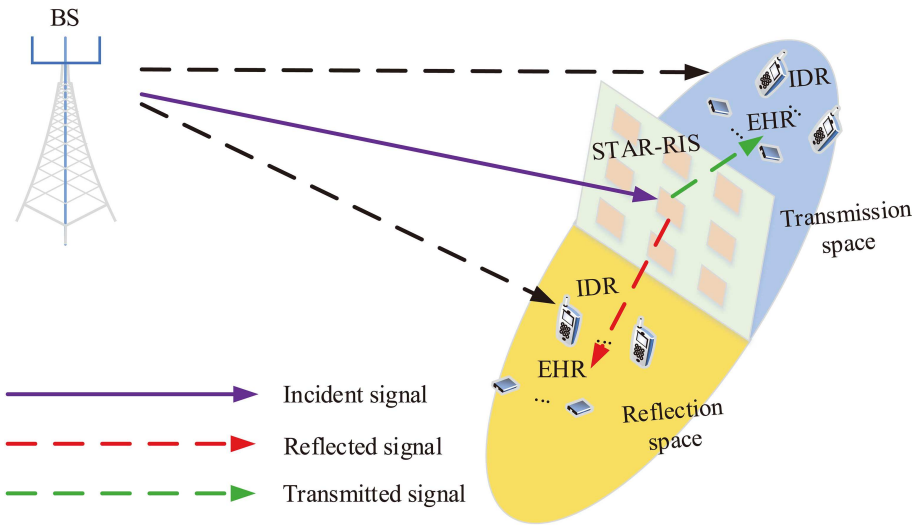

Figure 1 (Color online) STAR-RIS-aided SWIPT system.

and the elements of STAR-RIS are denoted as $\mathcal{K}, \mathcal{L}$, and $\mathcal{N}$, respectively. Different from the traditional RIS which only has the ability to reflect signals, STAR-RIS separates the communication space into the reflection and the transmission zones and realizes the full area coverage of signals. In order to comprehensively investigate the improvement of system performance by introducing a STAR-RIS [21], in this work, we study the SWIPT system supported by a STAR-RIS under three different protocols. Presumably, the signals that the n-th element transmits and reflects are represented by $t_n = \sqrt{\beta_n^t}\mathrm{e}^{\mathrm{j}\theta_n^t}$ and $r_n = \sqrt{\beta_n^r}\mathrm{e}^{\mathrm{j}\theta_n^r}$, respectively, where $\sqrt{\beta_n^t}, \sqrt{\beta_n^r} \in [0,1]$ stands for the amplitude and $\theta_n^t, \theta_n^r \in [0, 2\pi)$ for the phase shift of the n-th element.

Due to the independent control capability of STAR-RIS over transmitted and reflected signals, three different operating protocols can be achieved by adjusting the amplitude coefficient of transmission and reflection for each STAR-RIS element [21,22]. The three protocols of the STAR-RIS are defined as follows [21]. (1) ES protocol: each STAR-RIS element has the ability to transmit and reflect the incident signal concurrently. The magnitude of each element of STAR-RIS satisfies $\beta_n^t \geqslant 0, \beta_n^r \geqslant 0, \beta_n^t + \beta_n^r \leqslant 1$. Due to the ability to optimize the reflection and transmission coefficients of each element, the system design offers a high degree of freedom, resulting in a large number of optimization variables. (2) MS protocol: dividing all elements into two parts. One part contains N_1 elements for transmitting the incident signal, the other contains N_2 elements for reflecting the incident signal and $N_1 + N_2 = N$. Each element either works in transmission mode or in reflection mode. By using $a_n^p, p \in \{t, r\}$ to indicate whether the n-th element is in transmission mode or reflection mode, e.g., $a_n^t = 1, a_n^r = 0$ means the n-th element is in transmission mode, and $a_n^t = 0, a_n^r = 1$ means the n-th element is in reflection mode. The magnitude of each element at the STAR-RIS satisfies $a_n^p \in \{0,1\}, p \in \{t,r\}, a_n^t + a_n^r = 1, \beta_n^t \geqslant 0, \beta_n^r \geqslant 0, \beta_n^t \leqslant a_n^t, \beta_n^r \leqslant a_n^r$. In comparison to ES, this switching operation is easier to implement but has relatively lower transmission and reflection gains. (3) TS protocol: in separate orthogonal time slots, alternate between transmission and reflection modes on a periodic basis for each RIS element. The percentage of transmission period and reflection period to total communication time are $0 \leqslant \lambda_t \leqslant 1$ and $0 \leqslant \lambda_r \leqslant 1$, respectively, where $\lambda_t + \lambda_r = 1$. The magnitude of each element at the STAR-RIS satisfies $0 \leqslant \beta_n^t \leqslant 1, 0 \leqslant \beta_n^r \leqslant 1$. The decoupling of TARCs for a given time allocation allows for independent optimization of the coefficient matrices. However, periodic module switching imposes strict time synchronization requirements, leading to high hardware implementation complexity.

Furthermore, $\boldsymbol{\Psi}_p = \mathrm{diag}(\psi_{p,1}, \ldots, \psi_{p,N}), p \in \{t, r\}$ with $\psi_{p,n} = \sqrt{\beta_n^p}\mathrm{e}^{\mathrm{j}\theta_n^p}, n \in \mathcal{N}$ denoting its coefficient for the n-th element. The transmit signal at BS is denoted as $\boldsymbol{x} = \sum_{k=1}^{K} \boldsymbol{w}_k s_k$, where $s_k \sim \mathcal{CN}(0,1)$ represents desired data while $\boldsymbol{w}_k \in \mathbb{C}^{M\times 1}$ corresponds to transmit beamforming sent to k-th IDR. Considering the quasi-static flat-fading model for all channels, $\boldsymbol{G} \in \mathbb{C}^{N\times M}$, $\boldsymbol{h}_{\mathrm{IB},k}/\boldsymbol{h}_{\mathrm{IE},l} \in \mathbb{C}^{1\times N}$, and $\boldsymbol{h}_{\mathrm{AB},k}/\boldsymbol{h}_{\mathrm{AE},l} \in \mathbb{C}^{1\times M}$ represent channels from BS to STAR-RIS, from STAR-RIS to k-th IDR/l-th EHR, and from BS to k-th IDR/l-th EHR respectively. The channel state information (CSI) for STAR-RIS-aided systems can be obtained using existing channel estimation techniques [31,32]. The results presented in this work serve as a theoretical upper bound on system performance and offer guidance for system

design under imperfect CSI. Consequently, the received signals at k-th IDR and the l-th EHR are modeled as follows:

$$y_{b_p,k} = \boldsymbol{h}_{b_p,k}^{\mathrm{H}} \sum_{k=1}^{K} \boldsymbol{w}_k s_k + n_{b,k}, \tag{1}$$

$$y_{e_p,l} = \boldsymbol{h}_{e_p,l}^{\mathrm{H}} \sum_{k=1}^{K} \boldsymbol{w}_k s_k + n_{e,l}, \tag{2}$$

respectively, where $\boldsymbol{h}_{b_p,k}^{\mathrm{H}} = \boldsymbol{h}_{\mathrm{IB},k}^{\mathrm{H}} \boldsymbol{\Psi}_p \boldsymbol{G} + \boldsymbol{h}_{\mathrm{AB},k}^{\mathrm{H}} \in \mathbb{C}^{1\times M}$, $\boldsymbol{h}_{e_p,l}^{\mathrm{H}} = \boldsymbol{h}_{\mathrm{IE},l}^{\mathrm{H}} \boldsymbol{\Psi}_p \boldsymbol{G} + \boldsymbol{h}_{\mathrm{AE},l}^{\mathrm{H}} \in \mathbb{C}^{1\times M}, p \in \{t, r\}$, $n_b \sim \mathcal{CN}(0, \sigma_b^2)$ and $n_e \sim \mathcal{CN}(0, \sigma_e^2)$ are the complex additive white Gaussian noise (AWGN).

(1) ES and MS. When STAR-RIS applies ES protocol or MS protocol, the received SINR at the k-th IDR is

$$\mathrm{SINR}_{p,k}(\boldsymbol{w}_k, \boldsymbol{\Psi}_p) = \frac{|\boldsymbol{h}_{b_p,k}^{\mathrm{H}} \boldsymbol{w}_k|^2}{\sum_{j\neq k} |\boldsymbol{h}_{b_p,k}^{\mathrm{H}} \boldsymbol{w}_j|^2 + \sigma_{b,k}^2}, \quad p \in \{t, r\}. \tag{3}$$

Furthermore, the achieved rate at the k-th IDR is

$$R_{k_{\mathrm{EM}}}(\boldsymbol{w}_k, \boldsymbol{\Psi}_p) = \log_2(1 + \mathrm{SINR}_{p,k}(\boldsymbol{w}_k, \boldsymbol{\Psi}_p)), \quad p \in \{t, r\}. \tag{4}$$

At the l-th EHR, the RF power received is

$$P_{\mathrm{EH}_l}(\boldsymbol{w}_k, \boldsymbol{\Psi}_p) = \sum_{k=1}^{K} |\boldsymbol{h}_{e_p,l}^{\mathrm{H}} \boldsymbol{w}_k|^2, \quad p \in \{t, r\}. \tag{5}$$

(2) TS. When STAR-RIS applies TS protocol, the achieved rate at the k-th IDR is

$$R_{k_T}(\boldsymbol{w}_k, \boldsymbol{\Psi}_p, \lambda_p) = \lambda_p \log_2 \left(1 + \frac{|\boldsymbol{h}_{b_p,k}^{\mathrm{H}} \boldsymbol{w}_k|^2}{\sum_{j\neq k} |\boldsymbol{h}_{b_p,k}^{\mathrm{H}} \boldsymbol{w}_j|^2 + \sigma_k^2}\right), \quad p \in \{t, r\}. \tag{6}$$

The RF power received at the l-th EHR is

$$P_{\mathrm{EH}_l}(\boldsymbol{w}_k, \boldsymbol{\Psi}_p, \lambda_p) = \lambda_p \sum_{k=1}^{K} |\boldsymbol{h}_{e_p,l}^{\mathrm{H}} \boldsymbol{w}_k|^2, \quad p \in \{t, r\}. \tag{7}$$

Due to nonlinear features generated by components in actual energy harvesting circuits, end-to-end energy conversion cannot be adequately described using linear models [33]. For practical implementation, a nonlinear EH model is used, and the power gathered by the l-th EHR is represented by

$$E_l^{\mathrm{Non}} = (X_l - M_l \Omega_l)/(1 - \Omega_l), \tag{8}$$

where $X_l = \frac{M_l}{1+\exp\left(-a_l\left(P_{\mathrm{EH}_l} - b_l\right)\right)}$ is a logical function of the input RF signal power P_{EH_l} which is given in (5) and (7), X_l denotes the maximum value of energy that can be collected by the l-th EHR when the energy harvesting circuit is saturated, $\Omega_l = \frac{1}{1+\exp(a_l b_l)}$, a_l and b_l are specific parameters related to the energy harvesting circuit. The model adjusts three parameters, a_l, b_l, and M_l, to match the nonlinear characteristics caused by the actual circuit hardware constraints.

Considering the fairness of EHRs in collecting power, we maximize the WSP harvested by all EHRs. The WSP harvested by EHRs can be expressed as

$$E(\boldsymbol{w}_k, \boldsymbol{\Psi}_p) = \sum_{l=1}^{L} \omega_l E_l^{\mathrm{Non}}(\boldsymbol{w}_k, \boldsymbol{\Psi}_p), \quad \text{for ES/MS}, \tag{9}$$

$$E(\boldsymbol{w}_k, \boldsymbol{\Psi}_p, \lambda_p) = \sum_{l=1}^{L} \omega_l E_l^{\mathrm{Non}}(\boldsymbol{w}_k, \boldsymbol{\Psi}_p, \lambda_p), \quad \text{for TS}, \tag{10}$$

respectively, where $\omega_l \geqslant 0$ is the energy weight of the l-th EHR. A greater ω_l implies a higher priority for providing energy to the l-th EHR in comparison to other EHRs.

2.2 Problem formulation

Maximize the WSP received by all EHRs while satisfying the achieved rate constraints of all IDRs, the power constraints of the BS, and the per-element constraints of the STAR-RIS. To be more precise, the optimization problem for ES is

$$
\begin{aligned}
(\mathrm{P1}): \max_{\boldsymbol{w}_k, \boldsymbol{\Psi}_p} \quad & E(\boldsymbol{w}_k, \boldsymbol{\Psi}_p) && \text{(11a)}\\
\text{s.t.} \quad & R_{k_{\mathrm{EM}}}(\boldsymbol{w}_k, \boldsymbol{\Psi}_p) \geqslant \gamma_k, \forall k \in \mathcal{K}, && \text{(11b)}\\
& \sum_{k=1}^{K} \|\boldsymbol{w}_k\|^2 \leqslant P_s, && \text{(11c)}\\
& [\boldsymbol{\Psi}_p]_{n,n} = \sqrt{\beta_n^p} \mathrm{e}^{\mathrm{j}\theta_n^p},\ \theta_n^p \in [0, 2\pi),\ \forall n \in \mathcal{N}, && \text{(11d)}\\
& 0 \leqslant \beta_n^p \leqslant 1,\ \beta_n^t + \beta_n^r \leqslant 1,\ \forall n \in \mathcal{N}. && \text{(11e)}
\end{aligned}
$$

Different from ES STAR-RIS, each STAR-RIS component for MS operates in either reflection mode or transmission mode. Therefore, constraint (11e) cannot satisfy the MS STAR-RIS. To maximize the WSP collected by all EHRs, the optimization issue for MS STAR-RIS is defined as follows in light of its distinctive features:

$$
\begin{aligned}
(\mathrm{P2}): \max_{\boldsymbol{w}_k, \boldsymbol{\Psi}_p, \boldsymbol{a}_p} \quad & E(\boldsymbol{w}_k, \boldsymbol{\Psi}_p) && \text{(12a)}\\
\text{s.t.} \quad & \text{(11b)}, \text{(11c)}, \text{(11d)}, && \text{(12b)}\\
& a_n^p = \{0, 1\}, a_n^t + a_n^r = 1,\ \forall n \in \mathcal{N}, && \text{(12c)}\\
& \beta_n^p \geqslant 0,\ \beta_n^p \leqslant a_n^p,\ \forall n \in \mathcal{N}. && \text{(12d)}
\end{aligned}
$$

For TS, whether the incident signals are transmitted or reflected is controlled by the time parameter $\lambda_p, p \in \{t, r\}$, the weighted sum-harvesting power design is

$$
\begin{aligned}
(\mathrm{P3}): \max_{\boldsymbol{w}_k, \boldsymbol{\Psi}_p, \lambda_p} \quad & E(\boldsymbol{w}_k, \boldsymbol{\Psi}_p, \lambda_p) && \text{(13a)}\\
\text{s.t.} \quad & R_{k_T}(\boldsymbol{w}_k, \boldsymbol{\Psi}_p, \lambda_p) \geqslant \gamma_k, \quad \forall k \in \mathcal{K}, && \text{(13b)}\\
& [\boldsymbol{\Psi}_p]_{n,n} = \sqrt{\beta_n^p} \mathrm{e}^{\mathrm{j}\theta_n^p},\ \theta_n^p \in [0, 2\pi),\ \forall n \in \mathcal{N}, && \text{(13c)}\\
& \lambda_r \geqslant 0,\ \lambda_t \geqslant 0,\ \lambda_r + \lambda_t = 1, && \text{(13d)}\\
& \sum_{k=1}^{K} \lambda_p \|\boldsymbol{w}_k\|^2 \leqslant P_s, && \text{(13e)}\\
& 0 \leqslant \beta_n^t \leqslant 1,\ 0 \leqslant \beta_n^r \leqslant 1,\ \forall n \in \mathcal{N}. && \text{(13f)}
\end{aligned}
$$

In optimization problems (P1)–(P3), γ_k denotes the minimum achievable rate for the k-th IDR, P_s indicates the maximum TP provided by the BS[1)].

3 Joint beamforming and STAR-RIS coefficients design for ES

In this section, our main objective is to solve this intricate non-convex problem (P1) by optimizing both the transmit beamforming of BS and the TARCs of STAR-RIS. Because the optimization variables in the objective function are in exponential form and the objective function itself is in fractional form. Furthermore, a significant coupling exists between the optimization variables. This makes it challenging to solve the problem (P1) in its optimum or closed form using direct means. Considering both complexity in expression E_l^{Non} and our objective to maximize the sum of E_l^{Non} in the objective function, we first transform the objective function before solving the problem (P1). Here, the original problem is changed

1) Note that the response time of STAR-RIS and the signal processing time are crucial for the practicality of the proposed algorithm. However, this work primarily focuses on theoretical support for the system through rational algorithm design and does not currently involve hardware testing. We will also continue to monitor the research progress of STAR-RIS and integrate theoretical design with practical application in future endeavors.

into its matching equivalent optimization problem, which we then solve by introducing relaxation variables and employing the AO technique.

Specifically, according to the convex optimization theory [34], by introducing the relaxation variables $\eta_1, \ldots, \eta_L$ instead of $E_1^{\mathrm{Non}}, \ldots, E_L^{\mathrm{Non}}$ and adding the corresponding constraints, problem (P1) can be equivalently expressed as

$$
\begin{aligned}
(\mathrm{P1}'): \max_{\boldsymbol{w}_k, \boldsymbol{\Psi}_p, \eta_l} \ & \sum_{l=1}^{L} \omega_l \eta_l && \text{(14a)}\\
\text{s.t.} \ & E_l^{\mathrm{Non}}(\boldsymbol{w}_k, \boldsymbol{\Psi}_p) \geqslant \eta_l, \ \forall l \in \mathcal{L}, && \text{(14b)}\\
& R_{k_{\mathrm{EM}}}(\boldsymbol{w}_k, \boldsymbol{\Psi}_p) \geqslant \gamma_k, \ \forall k \in \mathcal{K}, && \text{(14c)}\\
& (11\mathrm{c}), (11\mathrm{d}), (11\mathrm{e}), && \text{(14d)}
\end{aligned}
$$

where (14b) are new constraints on E_l^{Non}. This ensures that problem (P1′) with the addition of auxiliary variables is equivalent to problem (P1).

Although the transformed objective function is already linear with respect to η_l, constraints (14b) and (14c) remain non-convex. Obviously, the optimization variables $\boldsymbol{w}_k$ and $\boldsymbol{\Psi}_p$ in constraints (14b) and (14c) are coupled and are present in the numerator and denominator. Therefore, solving problem (P1′) directly is tricky and it is difficult to obtain the optimal solution to problem (P1′). Following that, we perform the AO approach to generate the BS transmit beamforming and STAR-RIS coefficients, and then iterate over these two subproblems to produce a high-quality suboptimal solution of problem (P1′). The subproblems of optimizing $\boldsymbol{w}_k$ by fixing $\boldsymbol{\Psi}_p$ and optimizing $\boldsymbol{\Psi}_p$ by fixing $\boldsymbol{w}_k$ are described in detail below.

3.1 Optimize $\boldsymbol{w_k}$ with given $\boldsymbol{\Psi_p}$

With given $\boldsymbol{\Psi}_p$, problem (P1′) is reduced to

$$
\begin{aligned}
(\mathrm{P1\text{-}1}): \max_{\boldsymbol{w}_k, \eta_l} \ & \sum_{l=1}^{L} \omega_l \eta_l && \text{(15a)}\\
\text{s.t.} \ & E_l^{\mathrm{Non}}(\boldsymbol{w}_k) \geqslant \eta_l, \ \forall l \in \mathcal{L}, && \text{(15b)}\\
& R_{k_{\mathrm{EM}}}(\boldsymbol{w}_k) \geqslant \gamma_k, \ \forall k \in \mathcal{K}, && \text{(15c)}\\
& (11\mathrm{c}). && \text{(15d)}
\end{aligned}
$$

Note that E_l^{Non} is quadratic in relation to optimization variable $\boldsymbol{w}_k$, and E_l^{Non} appears in the denominator in exponential form. Furthermore, $R_{k_{\mathrm{EM}}}$ is quadratic in relation to optimization variable $\boldsymbol{w}_k$ which exists in both the numerator and the denominator. As a result, dealing directly with non-convex constraints (15b) and (15c) is tricky. To overcome this obstacle, we turn these non-convex constraints into convex ones by applying the first-order Taylor expansion approach combined with matrix equivalent transformation techniques. We next solve the subproblem (P1-1) by using the interior point strategy.

Constraint (15b) can be rewritten as

$$
P_{\mathrm{EH}_l}(\boldsymbol{w}_k) \geqslant b_l - \frac{\ln\left(\frac{M_l}{\eta_l + (M_l - \eta_l)\Omega_l} - 1\right)}{a_l}. \tag{16}
$$

It is significant to observe that Eq. (16) has a convex left-side in relation to $\boldsymbol{w}_k$ and a concave right-side with respect to η_l. We use the first-order Taylor expansion approach to the left-side of (16) in order to make (16) manageable as a convex constraint. As a result, $P_{\mathrm{EH}_l}(\boldsymbol{w}_k)$ can be represented as

$$
P_{\mathrm{EH}_l}(\boldsymbol{w}_k) \geqslant E_l(\boldsymbol{w}_k, \tilde{\boldsymbol{w}}_k), \tag{17}
$$

where $E_l(\boldsymbol{w}_k, \tilde{\boldsymbol{w}}_k) = \sum_{k=1}^{K} (2\Re\{\boldsymbol{w}_k^{\mathrm{H}} \boldsymbol{S} \tilde{\boldsymbol{w}}_k\} - \tilde{\boldsymbol{w}}_k^{\mathrm{H}} \boldsymbol{S} \tilde{\boldsymbol{w}}_k)$, $\boldsymbol{S} = \boldsymbol{h}_{e_p,l} \boldsymbol{h}_{e_p,l}^{\mathrm{H}}$. Eq. (17) is tight because $P_{\mathrm{EH}_l}(\boldsymbol{w}_k)$ is convex with respect to $\boldsymbol{w}_k$.

Moreover, the equation on the right side of inequality (16) may also be rewritten as

$$
b_l - \frac{\ln\left(\frac{M_l}{\eta_l + (M_l - \eta_l)\Omega_l} - 1\right)}{a_l} = b_l + \frac{-x_l(\eta_l)}{a_l} + \frac{y_l(\eta_l)}{a_l}, \tag{18}
$$

where $x_l(\eta_l) = \ln(M_l - \eta_l - (M_l - \eta_l)\,\Omega_l)$, $y_l(\eta_l) = \ln((1-\Omega_l)\eta_l + M_l\Omega_l)$. The second term in (18) is convex in relation to η_l, and the third term in (18) is concave in relation to η_l. Therefore, the third term in (18) needs to be transformed so that it is convex or linear in relation to η_l. The upper bound of $y_l(\eta_l)$, as per the first-order Taylor expansion technique, is

$$y_l(\eta_l) \leqslant \ln((1-\Omega_l)\tilde{\eta}_l + M_l\Omega_l) + \frac{1-\Omega_l}{(1-\Omega_l)\tilde{\eta}_l + M_l\Omega_l}(\eta_l - \tilde{\eta}_l) \triangleq \bar{y}_l(\eta_l, \tilde{\eta}_l). \tag{19}$$

Substituting (17)–(19) into (16), constraint (16) is transformed as

$$E_l(\boldsymbol{w}_k, \tilde{\boldsymbol{w}}_k) \geqslant b_l + \frac{-x_l(\eta_l)}{a_l} + \frac{\bar{y}_l(\eta_l, \tilde{\eta}_l)}{a_l}, \quad \forall l \in \mathcal{L}, \tag{20}$$

which is a convex constraint.

In addition, constraint (15c) can be rewritten as

$$|\boldsymbol{h}_{b_p,k}^{\mathrm{H}}\boldsymbol{w}_k|^2 \geqslant (2^{\gamma_k} - 1)\left(\sum_{j\neq k}|\boldsymbol{h}_{b_p,k}^{\mathrm{H}}\boldsymbol{w}_j|^2 + \sigma_{b,k}^2\right), \quad \forall k \in \mathcal{K}. \tag{21}$$

Due to the fact that $|\boldsymbol{h}_{b_p,k}^{\mathrm{H}}\boldsymbol{w}_k|^2$ is convex in relation to $\boldsymbol{w}_k$, utilizing the first-order Taylor expansion approach, the lower bound of $|\boldsymbol{h}_{b_p,k}^{\mathrm{H}}\boldsymbol{w}_k|^2$ is

$$|\boldsymbol{h}_{b_p,k}^{\mathrm{H}}\boldsymbol{w}_k|^2 \geqslant 2\Re\{\boldsymbol{w}_k^{\mathrm{H}}\boldsymbol{H}_{b,k}\tilde{\boldsymbol{w}}_k\} - \tilde{\boldsymbol{w}}_k^{\mathrm{H}}\boldsymbol{H}_{b,k}\tilde{\boldsymbol{w}}_k \triangleq B(\boldsymbol{w}_k, \tilde{\boldsymbol{w}}_k), \quad \forall k \in \mathcal{K}, \tag{22}$$

where $\boldsymbol{H}_{b,k} = \boldsymbol{h}_{b_p,k}\boldsymbol{h}_{b_p,k}^{\mathrm{H}}$. Consequently, non-convex constraint (15c) is converted, as seen below, into a convex constraint.

$$B(\boldsymbol{w}_k, \tilde{\boldsymbol{w}}_k) \geqslant (2^{\gamma_k} - 1)\left(\sum_{j\neq k}|\boldsymbol{h}_{b_p,k}^{\mathrm{H}}\boldsymbol{w}_j|^2 + \sigma_{b,k}^2\right), \quad \forall k \in \mathcal{K}. \tag{23}$$

Predicated on the previously mentioned conversions from (16) to (23), the subproblem (P1-1) could be transformed to

$$\text{(P1-1}'\text{)}: \max_{\boldsymbol{w}_k, \eta_l} \sum_{l=1}^{L}\omega_l\eta_l \qquad \text{s.t.} \ \ (20), (23), (11\text{c}). \tag{24}$$

Since all of the constraints in the problem (P1-1′) are convex and the objective function is linear in terms of η_l, this convex issue may be solved with the aid of tools like CVX [35].

3.2 Optimize $\boldsymbol{\Psi_p}$ with given $\boldsymbol{w_k}$

With given $\boldsymbol{w}_k$, problem (P1′) is reduced to

$$\begin{aligned}
\text{(P1-2)}: \max_{\boldsymbol{\Psi}_p, \eta_l} \ & \sum_{l=1}^{L}\omega_l\eta_l && \text{(25a)}\\
\text{s.t.} \ & E_l^{\mathrm{Non}}(\boldsymbol{\Psi}_p) \geqslant \eta_l, \ \forall l \in \mathcal{L}, && \text{(25b)}\\
& R_{k_{\mathrm{EM}}}(\boldsymbol{\Psi}_p) \geqslant \gamma_k, \ \forall k \in \mathcal{K}, && \text{(25c)}\\
& (11\text{d}), (11\text{e}). && \text{(25d)}
\end{aligned}$$

By defining $\boldsymbol{v}_p = [\psi_{p,1}, \ldots, \psi_{p,N}]$, $\boldsymbol{u}_p = [\boldsymbol{v}_p, 1]^{\mathrm{H}}$, $P_{\mathrm{EH}_l}(\boldsymbol{\Psi}_p)$ and $R_{k_{\mathrm{EM}}}(\boldsymbol{\Psi}_p)$ can be rewritten as [36]

$$P_{\mathrm{EH}_l}(\boldsymbol{u}_p) = \sum_{k=1}^{K}|\boldsymbol{u}_p^{\mathrm{H}}\boldsymbol{H}_{e,l}\boldsymbol{w}_k|^2, \ \forall l \in \mathcal{L} \tag{26}$$

and

$$R_{k_{\mathrm{EM}}}(\boldsymbol{u}_p) = \log_2\left(1 + \frac{|\boldsymbol{u}_p^{\mathrm{H}}\boldsymbol{H}_{b,k}\boldsymbol{w}_k|^2}{\sum_{j\neq k}|\boldsymbol{u}_p^{\mathrm{H}}\boldsymbol{H}_{b,k}\boldsymbol{w}_j|^2 + \sigma_b^2}\right), \tag{27}$$

Algorithm 1 AO algorithm for solving problem (P1′)

1: Initialization: $\boldsymbol{w}_k^{(0)}$,$\boldsymbol{\Psi}_p^{(0)}$, $n=0$, and convergence accuracy ϵ_1. The problem (P1′)'s objective value is indicated by $f^{(n)}$.
2: **repeat**
3: Calculate transmit beamforming $\boldsymbol{w}_k^{(n+1)}$ by solving problem (P1-1′) for given $\boldsymbol{\Psi}_p^{(n)}, p\in\{t,r\}$;
4: Calculate STAR-RIS coefficients $\boldsymbol{u}_p^{(n+1)}, p\in\{t,r\}$ by solving problem (P1-2′) for given $\boldsymbol{w}_k^{(n+1)}$;
5: Perform $\boldsymbol{\Psi}_p^{(n+1)}=\mathrm{diag}(\boldsymbol{u}_p^{(n+1)}),\ p\in\{t,r\}$;
6: Set $n=n+1$;
7: **until** $(f^{(n)}-f^{(n-1)})/(f^{(n)})\leqslant\epsilon_1$.

where $\boldsymbol{H}_{e,l}=[\mathrm{diag}(\boldsymbol{h}_{\mathrm{IE},l}^{\mathrm{H}})\boldsymbol{G};\boldsymbol{h}_{\mathrm{AE},l}^{\mathrm{H}}]$, $\boldsymbol{H}_{\mathrm{IE},l}=[\mathrm{diag}(\boldsymbol{h}_{\mathrm{IE},l}^{\mathrm{H}});\boldsymbol{0}]$, $\boldsymbol{H}_{b,k}=[\mathrm{diag}(\boldsymbol{h}_{\mathrm{IB},k}^{\mathrm{H}})\boldsymbol{G};\boldsymbol{h}_{\mathrm{AB},k}]$. Obviously, constraints (25b) and (25c) remain non-convex. Similar to Subsection 3.1, Eqs. (25b) and (25c) can be converted as

$$\boldsymbol{u}_p^{\mathrm{H}}\boldsymbol{\Xi}_l\boldsymbol{u}_p\geqslant 2\boldsymbol{u}_p^{\mathrm{H}}\boldsymbol{\Xi}_l\tilde{\boldsymbol{u}}_p-\tilde{\boldsymbol{u}}_p^{\mathrm{H}}\boldsymbol{\Xi}_l\tilde{\boldsymbol{u}}_p\triangleq E_l(\boldsymbol{u}_p,\tilde{\boldsymbol{u}}_p), \tag{28a}$$

$$E_l(\boldsymbol{u}_p,\tilde{\boldsymbol{u}}_p)\geqslant b_l+\frac{-x_l(\eta_l)}{a_l}+\frac{\bar{y}_l(\eta_l,\tilde{\eta}_l)}{a_l},\ \forall l\in\mathcal{L}, \tag{28b}$$

and

$$\boldsymbol{u}_p^{\mathrm{H}}\boldsymbol{Y}_k\boldsymbol{u}_p\geqslant 2\boldsymbol{u}_p^{\mathrm{H}}\boldsymbol{Y}_k\tilde{\boldsymbol{u}}_p-\tilde{\boldsymbol{u}}_p^{\mathrm{H}}\boldsymbol{Y}_k\tilde{\boldsymbol{u}}_p\triangleq A(\boldsymbol{u}_p,\tilde{\boldsymbol{u}}_p), \tag{29a}$$

$$A(\boldsymbol{u}_p,\tilde{\boldsymbol{u}}_p)\geqslant(2^{\gamma_k}-1)\left(\sum_{j\neq k}|\boldsymbol{u}_p^{\mathrm{H}}\boldsymbol{H}_{b,k}\boldsymbol{w}_j|^2+\sigma_b^2\right),\ \forall k\in\mathcal{K}, \tag{29b}$$

where $\boldsymbol{\Xi}_l=\sum_{k=1}^{K}\boldsymbol{H}_{e,l}\boldsymbol{w}_k\boldsymbol{w}_k^{\mathrm{H}}\boldsymbol{H}_{e,l}^{\mathrm{H}}$, $\boldsymbol{Y}_k=\boldsymbol{H}_{b,k}\boldsymbol{w}_k\boldsymbol{w}_k^{\mathrm{H}}\boldsymbol{H}_{b,k}^{\mathrm{H}}$.

Moreover, constraints (11d) and (11e) can be equivalently rewritten as

$$|u_n^t|^2\geqslant 0,\ |u_n^r|^2\geqslant 0,\ \forall n\in\mathcal{N}, \tag{30a}$$

$$|u_n^t|^2+|u_n^r|^2\leqslant 1,\ \forall n\in\mathcal{N}. \tag{30b}$$

Obviously, constraint (30a) is convex, however, constraint (30a) is non-convex. By performing first-order Taylor expansion, Eq. (30a) can be transformed as

$$2\Re\{u_n^p\tilde{u}_n^p\}-(\tilde{u}_n^p)^*\tilde{u}_n^p\geqslant 0,\ p\in\{t,r\},\ \forall n\in\mathcal{N}. \tag{31}$$

Subproblem (P1-2) can be changed as follows based on the aforementioned transformations:

$$(\text{P1-2}'):\max_{\boldsymbol{u}_p,\eta_l}\ \sum_{l=1}^{L}\omega_l\eta_l \tag{32a}$$

$$\text{s.t.}\ \ (28\text{b}),(29\text{b}),(30\text{b}),(31), \tag{32b}$$

$$|u_{N+1}^t|^2=1,|u_{N+1}^t|^2=1. \tag{32c}$$

Employing an interior point technique, the standard convex problem (P1-2′) may have its optimal solution found [34, 35]. The steps necessary to solve the problem are outlined in Algorithm 1.

4 Extension to MS STAR-RIS and TS STAR-RIS

We expand the alternating iterative optimization strategy presented in Section 3 to address problems (P2) and (P3) in this section. The two optimization issues pertaining to MS STAR-RIS and TS STAR-RIS are independently solved in the sections that follow.

4.1 Extended algorithm for MS STAR-RIS

The magnitude constraint of each element at the STAR-RIS distinguishes problem (P1) from problem (P2), which corresponds to the ES STAR-RIS theme and the MS STAR-RIS scheme, respectively. Problem (P2) is converted into an equivalent problem after the slack variables $\eta_l,\forall l\in\mathcal{L}$ are introduced and

the corresponding constraints for each EHR are added, similar to problem 1. The equivalent problem is

$$(\mathrm{P2}'): \max_{\boldsymbol{w}_k, \boldsymbol{\Psi}_p, \boldsymbol{a}_p, \eta_l} \sum_{l=1}^{L} \omega_l \eta_l \tag{33a}$$

$$\text{s.t.} \quad E_l^{\mathrm{Non}}(\boldsymbol{w}_k, \boldsymbol{\Psi}_p) \geqslant \eta_l, \ \forall l \in \mathcal{L}, \tag{33b}$$

$$(11\mathrm{b}), (11\mathrm{c}), (11\mathrm{d}), (12\mathrm{c}), (12\mathrm{d}). \tag{33c}$$

Obviously in problem (P2′), despite the objective function being linear in relation to η_l, the optimization variables in constraints (33b) and (11b) are coupled. In addition, constraint (12c) is a binary constraint with respect to the optimization variable $\boldsymbol{\Psi}_p$. These constraints are all non-convex and difficult to deal with directly. Therefore, we also perform the AO algorithm to solve the problem (P2′).

When $\boldsymbol{\Psi}_p$ is fixed, the reduced subproblem is the same as the problem (P1-1) and is omitted here. When $\boldsymbol{w}_k$ is fixed, problem (P2′) is reduced to

$$(\text{P2-1}'): \max_{\boldsymbol{\Psi}_p, \boldsymbol{a}_p, \eta_l} \sum_{l=1}^{L} \omega_l \eta_l \tag{34a}$$

$$\text{s.t.} \quad E_l^{\mathrm{Non}}(\boldsymbol{\Psi}_p) \geqslant \eta_l, \ \forall l \in \mathcal{L}, \tag{34b}$$

$$R_{k_{\mathrm{EM}}}(\boldsymbol{\Psi}_p) \geqslant \gamma_k, \ \forall k \in \mathcal{K}, \tag{34c}$$

$$(11\mathrm{d}), (12\mathrm{c}), (12\mathrm{d}). \tag{34d}$$

The transformation on (34b) and (34c) are the same as (28) and (29). The difficulty of problem (P2-1′) is the binary constraint (12c). To facilitate the calculation, it is first necessary to convert (12c) into a convex one. First, binary constraint (12c) can be presented equivalently as [37]

$$0 \leqslant a_n^p \leqslant 1, \ \forall n \in \mathcal{N}, \tag{35}$$

$$a_n^p - (a_n^p)^2 \leqslant 0, \ \forall n \in \mathcal{N}. \tag{36}$$

It is clear that constraint (35) is affine, whereas constraint (36) remains non-convex because of the presence of the quadratic term $(a_n^p)^2$. Given a feasible point $\tilde{a}_n^p$, constraint $(a_n^p)^2$ can be transformed into a linear constraint by employing a first-order Taylor expansion. However, if the first-order Taylor expansion is performed directly on constraint (36), the simultaneous existence of constraints (35) and (36) during the iteration may cause problem (P2-1) to be infeasible. The feasible domain of constraint (36) is first extended by introducing a set of slack variables $\boldsymbol{S} = s_n^p > 0, \forall n, p$ [37]. The objective function is then modified with a punishment term so that problem (P2-1′) can be reformulated as

$$(\text{P2-2}'): \max_{\boldsymbol{u}^p, \boldsymbol{a}^p, \eta_l, \boldsymbol{S}} \sum_{l=1}^{L} \omega_l \eta_l - \zeta \sum_{p} \sum_{n=1}^{N} s_n^p \tag{37a}$$

$$\text{s.t.} \quad (28\mathrm{b}), (29\mathrm{b}), (31), (35), \tag{37b}$$

$$\beta_n^p \leqslant a_n^p, \ \forall n \in \mathcal{N}, \tag{37c}$$

$$a_n^p - (a_n^p)^2 \leqslant s_n^p, \ \forall n \in \mathcal{N}, \tag{37d}$$

where $\zeta > 0$ is the penalty parameter. Since $s_n^p = 0, \forall n, p$ at the convergence point, problems (P2-1′) and (P2-2′) are equivalent. Therefore, it is guaranteed that $a_n^p = 0$ or $1, \forall n, p$ when problem (P2-2′) converges. Furthermore, by applying the first-order approximation technique, Eq. (37d) can be transformed into

$$(\tilde{a}_n^p)^2 + 2\tilde{a}_n^p(a_n^p - \tilde{a}_n^p) + s_n^p \geqslant a_n^p, \ \forall n, p. \tag{38}$$

By replacing constraint (37d) with constraint (38), problem (P2-2′) could be converted even further into

$$(\text{P2-3}'): \max_{\boldsymbol{u}^p, \boldsymbol{a}^p, \eta_l} \sum_{l=1}^{L} \omega_l \eta_l - \zeta \sum_{p} \sum_{n=1}^{N} s_n^p \tag{39a}$$

$$\text{s.t.} \quad (28\mathrm{b}), (29\mathrm{b}), (31), (37\mathrm{c}), (35), (38). \tag{39b}$$

Problem (P2-3′) is a standard convex function. The interior point approach can be used to solve this problem and obtain an optimal solution to the problem [34, 35]. Algorithm 2 provides a summary of the intricate algorithmic steps.

Algorithm 2 Penalty-based AO algorithm for solving problem (P2′)

Initialization: $\boldsymbol{w}_k^{(0)}$,$\boldsymbol{\Psi}_p^{(0)}$, convergence accuracy ϵ, the penalty factor ζ and set $n_1 = 0$. The problem (P2′)'s objective value is indicated by $f^{(n_1)}$.
repeat
  Calculate transmit beamforming $\boldsymbol{w}_k^{(n_1+1)}$ similar to problem (P1-1′);
  Set $n = 0$, convergence accuracy ϵ_1. Determine the problem (P2-3′)'s objective value and write it down as $f_2^{(n)}$;
  repeat
    Calculate STAR-RIS coefficients $\boldsymbol{u}_p^{(n+1)}, p \in \{t, r\}$ by solving problem (P2-3′);
    Set $\zeta = c\zeta$;
    Set $n = n + 1$;
  until $(f_2^{(n)} - f_2^{(n-1)})/(f_2^{(n)}) \leqslant \epsilon_1$;
  Set $n_1 = n_1 + 1$;
until $(f^{(n_1)} - f^{(n_1-1)})/(f^{(n_1)}) \leqslant \epsilon$.

4.2 Extended algorithm for TS STAR-RIS

Compared with problem (P1), problem (P3) adds new optimization variables $\lambda_p, p \in \{t, r\}$ in addition to the optimization variables $\boldsymbol{w}_k$ and $\boldsymbol{\Psi}_p$.

We add the necessary restrictions and create a sequence of auxiliary variables $\eta_l, \forall l \in \mathcal{L}$, just like in problem (P1), so that problem (P3) may be written as

$$(\text{P3}'): \max_{\boldsymbol{w}_k, \boldsymbol{\Psi}_p, \lambda_p, \eta_l} \sum_{l=1}^{L} \omega_l \eta_l \tag{40a}$$

$$\text{s.t.} \quad E_l^{\text{Non}}(\boldsymbol{w}_k, \boldsymbol{\Psi}_p, \lambda_p) \geqslant \eta_l, \ \forall l \in \mathcal{L}, \tag{40b}$$

$$(13\text{b}), (13\text{c}), (13\text{d}), (13\text{e}), (13\text{f}). \tag{40c}$$

To solve this complex optimization problem, the AO method is applied. When the variables λ_p is fixed, problem (P3′) is reduced as

$$(\text{P3-1}'): \max_{\boldsymbol{w}_k, \boldsymbol{\Psi}_p, \eta_l} \sum_{l=1}^{L} \omega_l \eta_l \tag{41a}$$

$$\text{s.t.} \quad E_l^{\text{Non}}(\boldsymbol{w}_k, \boldsymbol{\Psi}_p) \geqslant \eta_l, \forall l, \tag{41b}$$

$$(13\text{b}), (13\text{c}), (13\text{e}), (13\text{f}). \tag{41c}$$

Note that problem (P3-1′) is similar to problem (P1′), and the detailed solution procedure for problem (P3-1′) can be found in Section 3. When $\boldsymbol{w}_k$ and $\boldsymbol{\Psi}_p$ are fixed, the problem (P3′) may be reformulated and made simpler as follows:

$$(\text{P3-2}'): \max_{\lambda_p, \eta_l} \sum_{l=1}^{L} \omega_l \eta_l \tag{42a}$$

$$\text{s.t.} \quad R_{k_T}(\lambda_p) \geqslant \gamma_k, \quad \forall \ k \in \mathcal{K}, \tag{42b}$$

$$P_{\text{EH}_l}(\lambda_p) \geqslant b_l + \frac{-x_l(\eta_l)}{a_l} + \frac{\bar{y}_l(\eta_l, \tilde{\eta_l})}{a_l}, \quad \forall \ l \in \mathcal{L}, \tag{42c}$$

$$(13\text{d}), (13\text{e}). \tag{42d}$$

The objective function is linear in relation to the optimization variables λ_p and η_l, as are the constraints. Hence, problem (P3-2′) can be solved and obtained the optimal time allocation factor by CVX [35].

5 Convergence analysis and complexity analysis

The convergence and complexity of the three methods presented in the previous two sections are studied in this section, respectively.

5.1 Convergence analysis

For Algorithm 1, given a pair of feasible points $\{\boldsymbol{w}_k, \boldsymbol{\Psi}_p\}$, the objective value of problem (P1′) is denoted as $f(\boldsymbol{w}_k, \boldsymbol{\Psi}_p)$. According to steps 3 and 4 of Algorithm 1, we have $f(\boldsymbol{w}_k^{t+1}, \boldsymbol{\Psi}_p^t) \geqslant f(\boldsymbol{w}_k^t, \boldsymbol{\Psi}_p^t)$ and

$f(\boldsymbol{w}_k^{t+1}, \boldsymbol{\Psi}_p^{t+1}) \geqslant f(\boldsymbol{w}_k^{t+1}, \boldsymbol{\Psi}_p^{t})$, which are because that the optimal solutions are obtained for solving problem (P1-1′) and problem (P1-2′), respectively. Hence, we have this conclusion $f(\boldsymbol{w}_k^{t+1}, \boldsymbol{\Psi}_p^{t+1}) \geqslant f(\boldsymbol{w}_k^{t}, \boldsymbol{\Psi}_p^{t})$, which guarantees that the objective value of problem (P1′) does not decrease across iterations. Then, the target value of (P1′) is upper bounded because of the BS's power constraint and the IDRs's reachable rate constraint. Algorithm 1's convergence is therefore assured.

Similarly, for Algorithm 2, when $\boldsymbol{\Psi}_p$ is fixed, the optimal solution can be found. By resolving the problem (P2′), at least a locally optimum solution can be achieved. Thus, the objective value of Algorithm 2 shows monotonic non-decreasing behavior. Moreover, an upper bound on the problem (P2′)'s objective value exists. Therefore, there is also a guarantee that Algorithm 2 will converge. For problem (P3′), $f(\boldsymbol{w}_k^{t}, \boldsymbol{\Psi}_p^{t}, \eta^t) \leqslant f(\boldsymbol{w}_k^{t+1}, \boldsymbol{\Psi}_p^{t}, \eta^t) \leqslant f(\boldsymbol{w}_k^{t+1}, \boldsymbol{\Psi}_p^{t+1}, \eta^t) \leqslant f(\boldsymbol{w}_k^{t+1}, \boldsymbol{\Psi}_p^{t+1}, \eta^{t+1})$ due to each subproblem being solvable optimally and having an upper bound on the objective function value. Therefore, convergence of problem (P3′) is assured as well. Based on the aforementioned analysis and supported by simulation results in Section 4 demonstrating corresponding convergence behavior plots, it can be concluded that all three proposed algorithms are guaranteed to converge.

5.2 Complexity analysis

The complexity of solving problem (P1′) in Algorithm 1 is determined by the complexities involved in solving problem (P1-1′) and problem (P1-2′). Specifically, problem (P1-1′) consists of L linear matrix inequality (LMI) constraints with a size of $M+3$, K second-order cone (SOC) constraints with a dimension of 5, and 1 LMI constraint with a size of $M+1$. The complexity of resolving the problem (P1-1′) is therefore expressed as [38]

$$\begin{aligned}&\mathcal{O}_{E1}\Big(\sqrt{L(M+3)+(M+1)+2K}\big(n_1(L(M+3)^3+(M+1)^3)\\&+n_1^2(L(M+3)^2+(M+1)^2)+n_1(K5^2)+n_1^3\big)\Big),\end{aligned}\tag{43}$$

where $n_1 = \mathcal{O}(MK+L)$. Similarly, the complexity for solving problem (P1-2′) is [38]

$$\begin{aligned}&\mathcal{O}_{E2}\Big(\sqrt{L(N+3)+4N+2(K+N+2)}\big(n_2(L(N+3)^3+2N2^3)\\&+n_2^2(L(N+3)^2+2N2^2)+n_2(K5^2+N3^2+22^2)+n_2^3\big)\Big),\end{aligned}\tag{44}$$

where $n_2 = \mathcal{O}(2(N+1)+L)$. As a result, problem (P1′) has an overall complexity of $\mathcal{O}_1(D(\mathcal{O}_{E1}+\mathcal{O}_{E2}))$, where D is the number of iterations needed. Subproblem 1 for Algorithm 2 is identical to the problem (P1-1′). Furthermore, problem (P2-3′) has a computation complexity [38] of

$$\begin{aligned}&\mathcal{O}_{M2}\Big(D_{22}\sqrt{L(N+3)+4N+4+4N+6N+10K}\big(n_3(L(N+3)^3+2N2^3+22^3+4N+2N3^3)\\&+n_3(K5^2)+n_3^2(L(N+3)^2+2N2^2+22^2+4N+2N3^2)+n_3^3\big)\Big),\end{aligned}\tag{45}$$

where $n_3 = \mathcal{O}(2(N+1)+L+2N)$, D_{22} denotes the number of iterations in which problem (P2-3′) reaches convergence. Therefore, the overall complexity for solving problem (P2′) is $\mathcal{O}_2(D(\mathcal{O}_{E1}+\mathcal{O}_{M2}))$, where D stands for the number of iterations.

Similarly, for problem (P3′), with fixed λ_p, the computational complexity is the same as (43) and (44). With fixed $\boldsymbol{w}_k, \boldsymbol{\Psi}_p$, the computational complexity is

$$\mathcal{O}_{T3}\big(\sqrt{2K+3L+5}(n_{33}(K2^3+L3^3+3+2^3)+n_{33}^2(K2^2+L3^2+3+2^2)+n_{33}^3)\big),\tag{46}$$

where $n_{33} = \mathcal{O}(2+L)$. Therefore, the overall complexity for solving problem (P3′) is $\mathcal{O}_3(D(\mathcal{O}_{E1}+\mathcal{O}_{E2}+\mathcal{O}_{T3}))$, where D stands for the number of iterations.

6 Simulation results

This section presents numerical simulations to validate the system performance of a STAR-RIS-aided SWIPT. Four EHRs and four IDRs located in different areas with respect to STAR-RIS are taken into

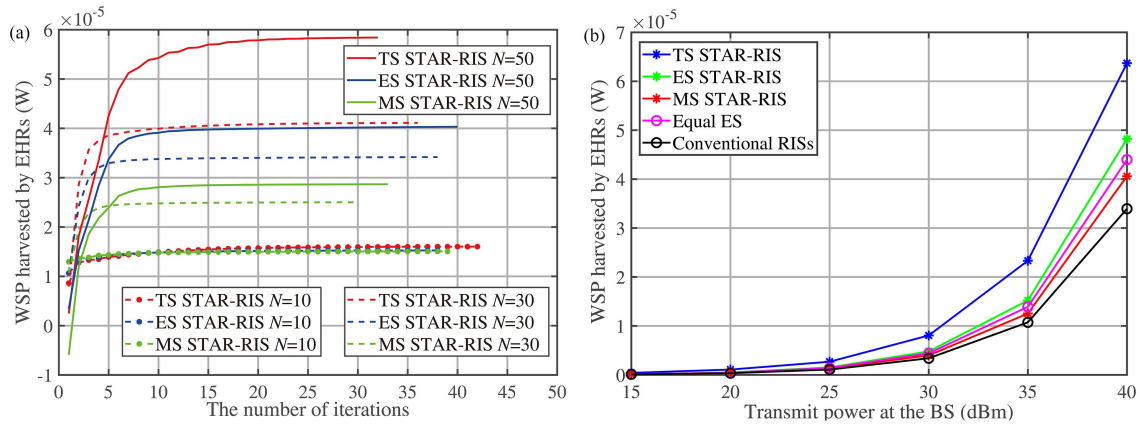

Figure 2 (Color online) (a) WSP harvested by EHRs vs. the number of iterations; (b) WSP harvested by EHRs vs. the TP at the BS.

account. The transmission zone of STAR-RIS contains two EHRs and two IDRs, whereas the reflection region of STAR-RIS has the other two EHRs and two IDRs. The BS and STAR-RIS are positioned at coordinates $(0, 0, 2)$ m and $(0, d_{yI}, 2)$ m, respectively. EHRs/IDRs in the STAR-RIS transmission zone are randomly distributed in a circle that is centered at $(0, d_{yI} + 3, 0)$ and has a radius of 2 m, while EHRs/IDRs in the reflection zone are distributed within another circle that is centered at $(0, d_{yI} - 3, 0)$ and has a radius of 2 m. In addition, the path loss model follows $P(d) = P_{d_0}(\frac{d}{d_0})^{-\alpha}$, where P_{d_0} indicates path loss at $d_0 = 1$ m, d is the link distance, and α is the path loss exponent. The path loss exponent between BS and EHRs/IDRs is $\alpha_{\mathrm{AB}} = \alpha_{\mathrm{AE}} = 3$, and this is a result of several barriers and scatterers that are present in the direct path that connects BS and EHRs/IDRs. The possibility of a feasible free-space path loss on a connection aided by STAR-RIS can be enhanced by carefully choosing the STAR-RIS position. Hence, the path loss exponent between BS and STAR-RIS and that between STAR-RIS and EHRs/IDRs are $\alpha_{\mathrm{AI}} = \alpha_{\mathrm{IB}} = \alpha_{\mathrm{IE}} = 2$.

In this work, Rician fading is used to represent small-scale fading, modeled as $\boldsymbol{h} = \sqrt{\rho/(\rho+1)}\boldsymbol{h}^{\mathrm{LoS}} + \sqrt{1/(\rho+1)}\boldsymbol{h}^{\mathrm{NLoS}}$, where ρ stands for the Rician factor, $\boldsymbol{h}^{\mathrm{LoS}}$ is the line-of-sight (LoS) part of the channel, and $\boldsymbol{h}^{\mathrm{NLoS}}$ is the Rayleigh fading, which is the non-line-of-sight (NLoS) part of the channel. Unless otherwise specified, there are $M = 8$ transmitting antennas at the BS and $N = 50$ STAR-RIS elements; the power at the BS is $P_s = 35$ dBm, and the distance of the STAR-RIS on the y-axis is $d_{yI} = 15$ m; the weighting factor is $\omega_l = 1, \forall l \in \mathcal{L}$, the minimum threshold of the achieved rate of IDRs is $\gamma_k = 2$ bit/s/Hz, $\forall k \in \mathcal{K}$, and the Rician factor is $\beta = 10$. The nonlinear energy harvesting model is associated with parameters $a_l = 150, b_l = 0.014, M_l = 0.02, \forall l \in \mathcal{L}$ [33] and noise power $\sigma_b^2 = -100$ dBm. To confirm the validity of the three proposed schemes of the STAR-RIS-aided SWIPT systems, we compare the following two benchmarks:

(1) Equal ES. Each STAR-RIS element transmits and reflects signals with a maximum amplitude of 0.5 concurrently.

(2) Conventional RISs. To provide full spatial coverage in this case, both a conventional reflection-only RIS and a transmission-only RIS can be applied. In the same location as STAR-RIS, these two traditional RISs are placed next to one another. Each reflection and transmission RIS has $N/2$ elements, where N is an even number, to allow for a fair comparison. Alternatively, one may consider this benchmark to be a particular case of MS STAR-RIS.

We initially verify the convergence performance of the STAR-RIS-aided systems under three protocols. Figure 2(a) displays the WSP that EHRs receive vs. the number of iterations of the proposed schemes under the three protocols when $N = 10, 30, 50$. It is evident from the figure that all three proposed schemes exhibit good convergence behavior. Even when N is relatively large, they converge within tens of iterations. Second, as N increases, the power collected by EHRs in the system under all three protocols increases. The reason for this is that more elements N lead to an increase in the degree of freedom for signal transmission, and stronger signals are transmitted or reflected into the EHRs through STAR-RIS. Moreover, among the three protocols, the EHRs in the TS STAR-RIS-aided systems collect the most WSP, followed by ES STAR-RIS and then MS STAR-RIS. This is because ES STAR-RIS and MS STAR-RIS send information to all users simultaneously, TS STAR-RIS transmits and reflects signals

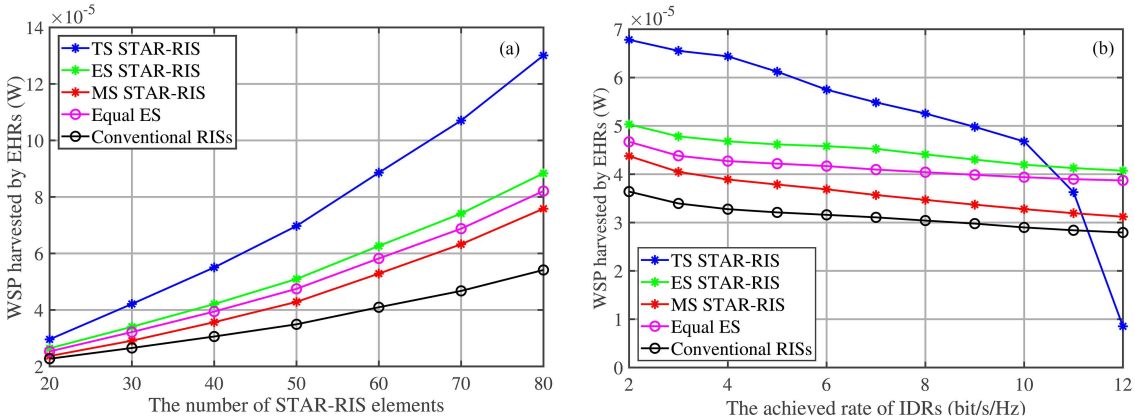

Figure 3 (Color online) (a) WSP harvested by EHRs vs. the number of STAR-RIS elements; (b) WSP harvested by EHRs vs. the achieved rate of IDRs.

through time division, and TS STAR-RIS creates less interference among users than ES STAR-RIS and MS STAR-RIS.

The WSP collected by EHRs vs. the TP at the BS is illustrated in Figure 2(b). The findings show that, in all cases, the WSP collected by EHRs grows as the TP budget increases. In all schemes, a higher TP budget leads to a greater amount of WSP collected by EHRs. Furthermore, it is evident from the figure that the STAR-RIS-aided system outperforms the traditional RIS-aided system, highlighting the capability of STAR-RIS deployment to enhance system performance. Notably, because of its stricter optimization range limiting amplitudes of transmission and reflection element within 0.5, equal ES performs more poorly than ES STAR-RIS. The EHRs in MS STAR-RIS, a unique instance of ES STAR-RIS, collect the least amount of power.

Figure 3(a) plots the WSP collected by EHRs vs. the number of STAR-RIS elements N. Apart from the three scenarios depicted, the outcomes of two baseline plans are offered for juxtaposition. Figure 3(a) shows that the WSP collected by EHRs grows with N for all schemes. This is because a greater N enables a stronger transmission and reflection beamforming gain, which further increases the collected energy of the EHRs. Of the three protocols proposed in this study, TS STAR-RIS has the best performance. This is because there is less interference between users in TS STAR-RIS than in the other schemes. Additionally, it is obvious that ES STAR-RIS performs better than MS STAR-RIS. This is expected because MS STAR-RIS is a special instance of ES STAR-RIS. The figure also shows that STAR-RIS performs better than conventional RISs as it can leverage more degrees of freedom to lower inter-user interference and boost desired signal strength, whereas conventional RISs are limited to using a specific number of transmission or reflection components. The performance comparison mentioned above attests to the suitability of STAR-RIS for application in wireless communication systems.

Figure 3(b) shows the WSP harvested by EHRs vs. the achieved rate of IDRs. The figure indicates that, in all cases, the WSP gathered by EHRs falls as the achieved rate of IDRs rises. This is because when the system TP is given, the higher the achieved rate of IDRs is, the more power IDRs need to receive, so the power received by EHRs decreases with it. Furthermore, TS STAR-RIS performs optimally when the achieved rate of IDRs is less than about 10.5 bit/s/Hz. Conversely, TS STAR-RIS underperforms compared to all other schemes when this rate exceeds 11 bit/s/Hz. This is because the lower communication interference in TS STAR-RIS comes at the cost of inefficient use of communication time, which becomes the primary performance barrier at the large achieved rate of IDRs. By contrast, ES STAR-RIS and MS STAR-RIS, along with both baseline schemes, serve all users throughout the communication time period. As a result, despite the presence of inter-user interference, their EHRs collect more energy than TS STAR-RIS under the higher achieved rate of IDRs. These results emphasize the importance of adopting different operating protocols for specific communication purposes and scenarios.

Figure 4(a) plots the harvested power at the EHRs vs. the distance of the STAR-RIS on the y-axis d_{yI} is plotted. The image shows that the power gathered by EHRs in all systems diminishes as d_{yI} increases. This is to be anticipated because d_{yI} grows as the distances between the EHRs and the BS and between the STAR-RIS and BS become bigger, the signal attenuation increases, and the power at the EHRs naturally declines. Furthermore, STAR-RIS-aided schemes outperform traditional RISs. Of

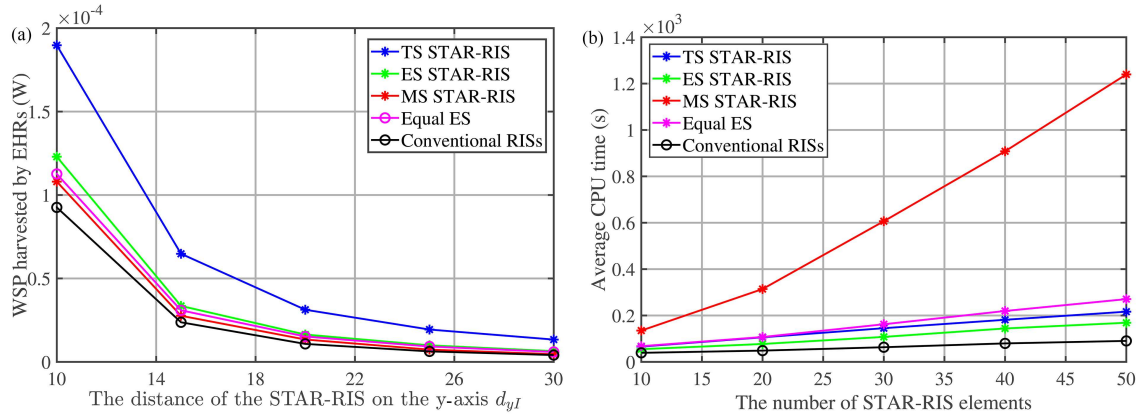

Figure 4 (Color online) (a) WSP harvested by EHRs vs. the distance of the STAR-RIS on the y-axis d_{yI}; (b) average CPU time vs. the number of STAR-RIS elements.

the three protocols that correlate to STAR-RIS, TS STAR-RIS has the best performance, followed by ES STAR-RIS and MS STAR-RIS. The graph also demonstrates that the STAR-RIS-aided system may put EHRs more widely than the traditional RIS-aided system for the same amount of power gathered by the EHRs.

Figure 4(b) illustrates the average central processing unit (CPU) time of the three proposed schemes vs. the number of STAR-RIS elements N. First, the figure shows that as N grows, the average CPU time needed for all schemes increases. This is because an increase in N causes the RIS coefficient optimization variables to become larger and the algorithms to converge more slowly. Second, the figure also shows that MS STAR-RIS takes the most CPU time, which is caused by binary constraints in the algorithm that correspond to the MS protocol. Moreover, TS STAR-RIS takes much less CPU time than MS STAR-RIS and slightly more than ES STAR-RIS. This is because the algorithm that corresponds to ES STAR-RIS needs to compute two subproblems by performing the alternate iteration method until the objective function converges, while the algorithm that corresponds to TS STAR-RIS needs to perform similar calculations for three subproblems.

7 Conclusion

This paper investigated a nonlinear energy harvesting model-based SWIPT system assisted by a STAR-RIS through which signals are transmitted and reflected. To maximize the WSP gathered at all EHRs under three protocols, joint optimization of transmit beamforming at the BS and TARCs at the STAR-RIS was performed, subject to rate constraints of IDRs, TP constraint at BS, and coefficient constraints of STAR-RIS. However, it was discovered that these problems were non-convex and intractable because of the complexity brought about by the strongly linked optimization variables and the nonlinear energy harvesting model objective function. For the ES STAR-RIS scheme, the AO algorithm was used to solve non-convex problems based on matrix equivalent transformation and the first-order approximation technique. For the MS STAR-RIS scheme, the RIS coefficient optimization subproblem was a 0-1 integer programming problem. The solution to the subproblem was obtained using a first-order Taylor expansion technique and a penalty mechanism. Finally, the AO method that corresponds to the ES STAR-RIS scheme was extended to the TS STAR-RIS scheme with a suboptimal solution obtained for the optimization problem that corresponds to TS. Numerical simulation results showed that the proposed schemes significantly outperform traditional RIS-aided systems.

Acknowledgements This work was supported in part by National Natural Science Foundation of China (Grant Nos. U22A2002, 62071234), Hainan Province Science and Technology Special Fund (Grant No. ZDKJ2021022), Scientific Research Fund Project of Hainan University (Grant No. KYQD(ZR)-21008), Collaborative Innovation Center of Information Technology, Hainan University (Grant No. XTCX2022XXC07), and Key Special Project of Technology from Nanjing City Government, China (Grant No. 202309010).

References

1 Huang C, Hu S, Alexandropoulos G C, et al. Holographic MIMO surfaces for 6G wireless networks: opportunities, challenges, and trends. IEEE Wireless Commun, 2020, 27: 118–125

2 Chen X, Ng D W K, Chen H H. Secrecy wireless information and power transfer: challenges and opportunities. IEEE Wireless Commun, 2016, 23: 54–61
3 Shi B, Jiang X, Chen N, et al. Fast ambiguous DOA elimination method of DOA measurement for hybrid massive MIMO receiver. Sci China Inf Sci, 2022, 65: 159302
4 Wan Z Q, Pan Q J, Li J M, et al. Performance analysis of full-duplex densely distributed MIMO with wireless backhaul. Sci China Inf Sci, 2023, 66: 162303
5 Shi W, Wu Q, Xiao F, et al. Secrecy throughput maximization for IRS-aided MIMO wireless powered communication networks. IEEE Trans Commun, 2022, 70: 7520–7535
6 Xu J, Liu L, Zhang R. Multiuser MISO beamforming for simultaneous wireless information and power transfer. IEEE Trans Signal Process, 2014, 62: 4798–4810
7 Zhou X, Li J, Shu F, et al. Secure SWIPT for directional modulation-aided AF relaying networks. IEEE J Sel Areas Commun, 2019, 37: 253–268
8 Li B, Fei Z S. Probabilistic-constrained robust secure transmission for energy harvesting over MISO channels. Sci China Inf Sci, 2018, 61: 022303
9 Liu L, Zhang R, Chua K C. Secrecy wireless information and power transfer with MISO beamforming. IEEE Trans Signal Process, 2014, 62: 1850–1863
10 Shu F, Qin Y, Liu T, et al. Low-complexity and high-resolution DOA estimation for hybrid analog and digital massive MIMO receive array. IEEE Trans Commun, 2018, 66: 2487–2501
11 Wu Y, Wen C K, Chen W, et al. Data-aided secure massive MIMO transmission under the pilot contamination attack. IEEE Trans Commun, 2019, 67: 4765–4781
12 Wu Q, Zhang R. Intelligent reflecting surface enhanced wireless network via joint active and passive beamforming. IEEE Trans Wireless Commun, 2019, 18: 5394–5409
13 Shu F, Yang L, Jiang X, et al. Beamforming and transmit power design for intelligent reconfigurable surface-aided secure spatial modulation. IEEE J Sel Top Signal Process, 2022, 16: 933–949
14 Peng Z J, Liu X Y, Liu X, et al. Performance analysis of active RIS-aided multi-pair full-duplex communications with spatial correlation and imperfect CSI. Sci China Inf Sci, 2023, 66: 192304
15 Shi W, Li J, Xia G, et al. Secure multigroup multicast communication systems via intelligent reflecting surface. China Commun, 2021, 18: 39–51
16 Wu Q, Guan X, Zhang R. Intelligent reflecting surface-aided wireless energy and information transmission: an overview. Proc IEEE, 2022, 110: 150–170
17 Shu F, Teng Y, Li J, et al. Enhanced secrecy rate maximization for directional modulation networks via IRS. IEEE Trans Commun, 2021, 69: 8388–8401
18 Wu Q, Zhang R. Towards smart and reconfigurable environment: intelligent reflecting surface aided wireless network. IEEE Commun Mag, 2020, 58: 106–112
19 Shen H, Xu W, Gong S, et al. Secrecy rate maximization for intelligent reflecting surface assisted multi-antenna communications. IEEE Commun Lett, 2019, 23: 1488–1492
20 Hua M, Wu Q, Ng D W K, et al. Intelligent reflecting surface-aided joint processing coordinated multipoint transmission. IEEE Trans Commun, 2021, 69: 1650–1665
21 Liu Y, Mu X, Xu J, et al. STAR: Simultaneous transmission and reflection for 360° coverage by intelligent surfaces. IEEE Wireless Commun, 2021, 28: 102–109
22 Mu X, Liu Y, Guo L, et al. Simultaneously transmitting and reflecting (STAR) RIS aided wireless communications. IEEE Trans Wireless Commun, 2022, 21: 3083–3098
23 Wu C, Liu Y, Mu X, et al. Coverage characterization of STAR-RIS networks: NOMA and OMA. IEEE Commun Lett, 2021, 25: 3036–3040
24 Wu Q, Zhang R. Joint active and passive beamforming optimization for intelligent reflecting surface assisted SWIPT under QoS constraints. IEEE J Sel Areas Commun, 2020, 38: 1735–1748
25 Wu Q, Zhang R. Weighted sum power maximization for intelligent reflecting surface aided SWIPT. IEEE Wireless Commun Lett, 2020, 9: 586–590
26 Pan C, Ren H, Wang K, et al. Intelligent reflecting surface aided MIMO broadcasting for simultaneous wireless information and power transfer. IEEE J Sel Areas Commun, 2020, 38: 1719–1734
27 Shi W, Zhou X, Jia L, et al. Enhanced secure wireless information and power transfer via intelligent reflecting surface. IEEE Commun Lett, 2021, 25: 1084–1088
28 Hehao N, Ni L. Intelligent reflect surface aided secure transmission in MIMO channel with SWIPT. IEEE Access, 2020, 8: 192132
29 Xu J, Liu Y, Mu X, et al. STAR-RISs: simultaneous transmitting and reflecting reconfigurable intelligent surfaces. IEEE Commun Lett, 2021, 25: 3134–3138
30 Han Y, Li N, Liu Y, et al. Artificial noise aided secure NOMA communications in STAR-RIS networks. IEEE Wireless Commun Lett, 2022, 11: 1191–1195
31 Wu C, You C, Liu Y, et al. Channel estimation for STAR-RIS-aided wireless communication. IEEE Commun Lett, 2022, 26: 652–656
32 Khalid W, Kaleem Z, Ullah R, et al. Simultaneous transmitting and reflecting-reconfigurable intelligent surface in 6G: design guidelines and future perspectives. IEEE Netw, 2023, 37: 173–181
33 Zeng P, Wu Q, Qiao D. Energy minimization for IRS-aided WPCNs with non-linear energy harvesting model. IEEE Wireless Commun Lett, 2021, 10: 2592–2596
34 Boyd S, Vandenberghe L. Convex Optimization, Cambridge: Cambridge University Press, 2004
35 Grant M, Boyd S. CVX: MATLAB software for disciplined convex programming. 2014. http://cvxr.com/cvx
36 Zhang X D. Matrix Analysis and Applications. Cambridge: Cambridge University Press, 2017
37 Lu J, Wang Y, Liu T, et al. UAV-enabled uplink non-orthogonal multiple access system: joint deployment and power control. IEEE Trans Veh Technol, 2020, 69: 10090–10102
38 Wang K Y, So A M C, Chang T H, et al. Outage constrained robust transmit optimization for multiuser MISO downlinks: tractable approximations by conic optimization. IEEE Trans Signal Process, 2014, 62: 5690–5705